



# Random forest-based prediction of decay modes and half-lives of superheavy nuclei

Bo-Shuai Cai<sup>1</sup> · Cen-Xi Yuan<sup>1</sup>

Received: 18 July 2023 / Revised: 3 September 2023 / Accepted: 13 September 2023 / Published online: 13 December 2023

© The Author(s), under exclusive licence to China Science Publishing & Media Ltd. (Science Press), Shanghai Institute of Applied Physics, the Chinese Academy of Sciences, Chinese Nuclear Society 2023

## Abstract

Information on the decay process of nuclides in the superheavy region is critical in investigating new elements beyond oganesson and the island of stability. This paper presents the application of a random forest algorithm to examine the competition among different decay modes in the superheavy region, including  $\alpha$  decay,  $\beta^-$  decay,  $\beta^+$  decay, electron capture and spontaneous fission. The observed half-lives and dominant decay mode are well reproduced. The dominant decay mode of 96.9% of the nuclei beyond  $^{212}\text{Po}$  is correctly obtained. Further,  $\alpha$  decay is predicted to be the dominant decay mode for isotopes in new elements  $Z = 119 - 122$ , except for spontaneous fission in certain even–even elements owing to the increased Coulomb repulsion and odd–even effect. The predicted half-lives demonstrate the existence of a long-lived spontaneous fission island southwest of  $^{298}\text{Fl}$  caused by the competition between the fission barrier and Coulomb repulsion. A better understanding of spontaneous fission, particularly beyond  $^{286}\text{Fl}$ , is crucial in the search for new elements and the island of stability.

**Keywords** Decay mode · Superheavy nuclide · Random forest

## 1 Introduction

Limitations of the nuclear landscape [1, 2] have always been an intriguing topic. Exotic nuclear properties, for example, the shell evolution [3–6],  $4n$  resonant state [7, 8], and  $4p$  unbound state [9], emerge at the limits of nuclear stability. The discovery of new elements (nuclides) involves the following three problems: production, separation, and identification [10]. Because the nuclei are unstable and have relatively short half-lives, appropriate probes must be utilized. Characteristic decay modes [10, 11] are commonly employed as a probe to signal the existence of exotic nuclei. Therefore, investigating and predicting the dominant decay modes of the unknown nuclides is crucial. The nuclear

binding energy and half-life are key parameters for determining the decay mode of a nucleus. The former measures the stability of nuclides by using energy criteria, and the latter describes the possibility of decay.

Both microscopic and macroscopic methods have been used to study the nuclear binding energy [12–16] and partial half-life of each decay channel, including  $\alpha$  decay [17–19],  $\beta$  decay [20, 21], spontaneous fission [22, 23], protons emission [25] and neutron emission [24], etc. Microscopic theories begin with nucleon–nucleon interactions, which can be based on either realistic or phenomenological models. The macroscopic theory uses selected variables with physical considerations to construct semi-empirical formulas and fit the experimental data, and it entails the risk of overfitting and inappropriate parameters. In addition, exotic nuclei may significantly deviate from the general fitting and be identified as outliers. Decreasing the deviation between theoretical predictions and the observed results remains a critical issue.

With advances in computing and storage, efficacious machine learning algorithms with diverse applications have been proposed [26, 27], e.g., nuclear properties [28–30], fission yields [31–35], spectra decomposition [36], solving Schrödinger equation [37], and other nuclear techniques [38, 39]. As summarized in a recent colloquium, estimating

---

This work was supported by the Guangdong Major Project of Basic and Applied Basic Research under Grant No. 2021B0301030006, and the computational resources from SYSU and the National Supercomputer Center in Guangzhou.

---

✉ Cen-Xi Yuan  
yuancx@mail.sysu.edu.cn

<sup>1</sup> Sino-French Institute of Nuclear Engineering and Technology, Sun Yat-sen University, Zhuhai 519082, China

the residuals of nuclear properties using machine learning algorithms is a powerful strategy [40]. A neural network has been used to compensate for the residuals of nuclear masses [41–43] and nuclear charge radii [44–46]; this has been achieved through structural optimization and careful selection of the input parameters with definite physical interpretations. The applicability of the decision tree (DT) has been verified via training and testing with residuals of the binding energies [47]. However, random forest (RF) [48] algorithm, developed from the DT algorithm, has not been tested for determining the nuclear mass or the partial half-life of a specific decay channel; in this regard, semi-empirical formulas have suggested several major components but with residuals. Machine learning algorithms can include possible features to realize the training for residuals, whereas RF, with bootstrap sampling, not only avoids overfitting but also considers the correlation between the data combinations and several features. Thus, RF exhibits increased robustness and is conducive to extrapolation. The amount of computation increasing in accordance with the number of trees in the forest and size of the dataset, as well as the difficulty of model interpretability, may limit its applications.

This study entailed the application of an RF machine learning algorithm to analyze the major decay modes of heavy and superheavy nuclei. The competition between  $\alpha$  decay,  $\beta$  decay, and spontaneous fission (SF) of new elements, as well as the possible long-lived island in the superheavy region, was examined.

## 2 Method

This study focused on the  $Z \geq 84$  and  $N \geq 128$  regions. The partial half-lives of the  $\alpha$  decay,  $\beta^-$  decay,  $\beta^+$  decay, electron capture (EC), and SF were calculated using semi-empirical formulas, and the residuals of each formula were then trained using the RF algorithm. The minimum partial half-life of a mode corresponds to the dominant decay mode.

### 2.1 Decay half-life formulas

The universal decay law (UDL) [49, 50],

$$\log_{10} T_{1/2,\alpha} = aZ_\alpha(Z - Z_\alpha)\sqrt{\mu/Q_\alpha} + b\sqrt{\mu Z_\alpha(Z - Z_\alpha)(A_\alpha^{1/3} + (A - A_\alpha)^{1/3})} + c, \tag{1}$$

is used to fit the  $\alpha$ -decay half-life.  $Z_\alpha$ ,  $A_\alpha$ ,  $Q_\alpha$ , and  $\mu = A_\alpha(A - A_\alpha)/A$  denote the proton number, mass number of the  $\alpha$  particle,  $\alpha$  decay energy, and reduced mass, respectively. The decay channel is assumed to move from the ground state to the ground state.

A three-parameter formula (denoted as SF3) was used for the SF as follows:

$$\log_{10} T_{\text{SF}} = a \frac{(Z - \nu)^2}{(1 - \kappa I^2)A} + \frac{b}{A} + c, \tag{2}$$

which was proposed based on several existing formulas [22, 23, 51–54], where  $\nu$  represents the blocking effect from unpaired nucleons; its value is 0 for even–even nuclei and 2 for other nuclei [51].  $\kappa$  has a value of 2.6 [22, 55],  $I = \frac{N-Z}{A}$ , and  $a$ ,  $b$ , and  $c$  are the fitting coefficients. Eq (2) is separately fitted to nuclei with  $Z < 104$  and the remaining because of a systematic difference, as shown in Table 1.  $T_{1/2,\text{SF}}$  of the nuclei with  $Z < 104$  increases significantly with a decrease in  $Z$  because the Coulomb repulsion decreases. The relatively long  $T_{\text{SF}} (> 10^8 \text{ s})$  of certain nuclei in this region cannot be universally described currently and were not used to fit Eq.(2) because the competition for the SF is significantly weak compared to other decay modes.

The  $\beta$  decay half-life was estimated using the formula given in Refs. [21, 56]. Assuming that the ground state  $\beta$  decay is an effective Gamow–Teller (GT) transition, the partial half-life can be expressed as follows:

$$\log_{10} T_{1/2,\beta} = \log_{10} \kappa_1 - \log_{10} f_0 - \log_{10} B_{\text{GT}}, \tag{3}$$

**Table 1** Coefficients and corresponding root-mean-square error (RMSE) of the UDL, SF3, and Eq. (3) when fitted to the nuclei with  $Z \geq 84$  &  $N \geq 128$

	$a$ ( $\log_{10} B_{\text{GT}}$ )	$b$	$c$	RMSE	RMSE <sub>RF,WS4</sub>	RMSE <sub>RF,UNEDF0</sub>
UDL	0.407	−0.382	−23.896	0.883	0.598	0.669
SF3 ( $Z < 104$ )	−1.129	−6997.113	79.803	3.070	1.195	1.195
SF3 ( $Z \geq 104$ )	−1.363	−13272.729	113.415	1.267	0.825	0.825
Eq. (3) <sub><math>\beta^+</math></sub>	1.378	–	–	1.957	0.439	0.437
Eq. (3) <sub><math>\beta^-</math></sub>	−1.819	–	–	1.451	0.656	0.667
Eq. (3) <sub>EC</sub>	−2.112	–	–	2.360	0.971	0.996

The RMSEs of the RF-trained UDL, SF3, and Eq. (3) are listed in the last two columns. The Weizsäcker–Skyrme (WS4) [12] and universal nuclear energy density functional (UNEDF0) [13] in the subscript indicate the sources of predicted energies

where  $\kappa_1 = \frac{2\pi^3 \hbar^7 \ln 2}{m_e^5 c^4 G_F^2} = 6147$  s,  $f_0$  is the phase-space factor, and  $B_{GT}$  is the GT-reduced transition probability [56]. As regards EC, the phase-space factor is deduced as follows:

$$f_0^{EC} \approx 2\pi \left(\frac{Z}{137}\right)^3 \left(1 - \frac{1}{2} \left(\frac{Z}{137}\right)^2 + E_0\right)^2, \tag{4}$$

whereas for the  $\beta^\pm$  decay, it is

$$f_0^{\beta^\pm} \approx \frac{\mp(E_0^5 - 10E_0^2 + 15E_0 - 6)2\pi(Z \mp 1)/137}{30(1 - \exp(\pm 2\pi(Z \mp 1)/137))}, \tag{5}$$

where  $E_0$  is the renormalized  $\beta$ -decay energy. Because  $Q_\beta$  provided by AME2020 [57] is the difference in the atomic mass, the electron mass should be reconsidered as follows:

$$\begin{aligned} E_{0,\beta^+} &= \frac{Q_{\beta^+} + 2m_e c^2}{m_e c^2} \\ E_{0,\beta^-} &= \frac{Q_{\beta^-} + m_e c^2}{m_e c^2} \\ E_{0,EC} &= \frac{Q_{EC} - m_e c^2}{m_e c^2}. \end{aligned} \tag{6}$$

Finally,  $\log_{10} B_{GT}$  is estimated as the average  $\log_{10}(f_0 T_{1/2,\beta}/\kappa_1)$ . The fitting results are listed in Table 1.

### 2.2 Random forest method

RF is a fusion of the DT and bootstrap algorithms. DT is a nonparametric supervised learning algorithm. For a dataset consisting of  $S$  samples of  $I$  features (variables)  $\{(\theta_1, \dots, \theta_I)_s, s \in [1, S]\}$  and object (observable)  $\{y_s, s \in [1, S]\}$ , it establishes a binary tree structure that divides the dataset into  $L$  subsets based on the values of the features; each subset is called a leaf. This partition seeks to minimize the RMSE

$$RMSE = \sqrt{\frac{1}{S} \sum_{s=1}^S (y_s - f(\theta_1, \dots, \theta_I))^2} \tag{7}$$

of the entire dataset by assigning a value to each leaf.

Bootstrap is a statistical method based on the concept of random resampling with replacement, through which possible combinations and weights of data are automatically considered [58, 59]. Each time a new dataset is obtained, a new DT is trained and used to predict the object of each sample in the entire dataset. By repeating this process  $M$  times, a forest of  $M$  trees is obtained. The final predicted value of the object for a sample is the average of the results calculated by all the trees in the forest. Because each tree is trained by part of the samples in the dataset, the value for each sample predicted by the forest is an average of the interpolation and

extrapolation; this decreases the divergence when the calculation is implemented for the unmeasured nuclei. The open-source Python library scikit-learn [60] was used for machine learning. The forest was assumed to be composed of  $10^5$  trees so as to decrease the dispersion of the RMSE in this study.

### 3 Results and discussion

The residuals of the decay formulas of  $\alpha$  decay,  $\beta^-$  decay,  $\beta^+$  decay, and EC were trained using the RF with features  $Z, N, A$ , the oddity of  $Z$  and  $N$ , and the decay energy. Because the decay energy cannot be defined for the SF, the fission barrier (FB) obtained from Ref. [61] was used to replace the decay energy in the feature set to consider the deformation effect. The number of leaves chosen for this study was 11, which was the same as that used for training the binding energy in this region in our previous study [62]. Figure 1 compares the residuals of these decay formulas before and after RF training. Two conditions were assumed to determine the outliers: 1) located outside the dashed line with the corresponding color, which indicates that the scatter deviates by twice the RMSE from the experimental  $\log_{10} T_{1/2}$ ; and 2) the  $|\log_{10}(T_{1/2,cal}/T_{1/2,exp})|$  value is larger than 3, which indicates that the calculated value is three times that of the magnitude of the experimental value. Thus, missing (adding) the outliers owing to the significantly large (small) RMSE can be avoided.

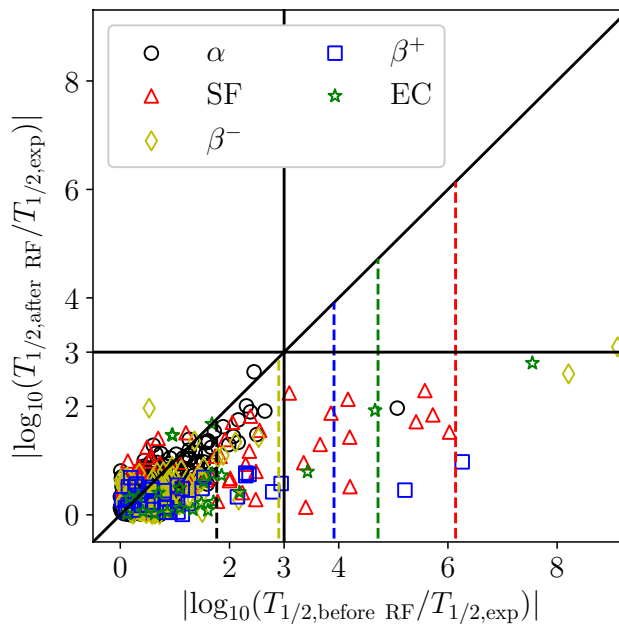


Fig. 1 (Color online) Comparison of the residuals of UDL ( $\alpha$  decay), SF3 (SF), Eq. (3) ( $\beta^-$ ,  $\beta^+$  and EC) before and after RF training. The dashed lines denote twice the RMSE of the corresponding formulas

After training, the biases of the outliers of these decay formulas were significantly reduced, and the RMSE of the formulas decreased (Table 1), as expected. The condition of the outlier is not too strict because the aim was not to maximally decrease the RMSE but to reach an appropriate scale, wherein the dominant decay mode can be described. The same features and number of leaves of the RF were chosen in this study to train the residuals of the different decay formulas; this avoids overfitting while seeking an extremely small RMSE.

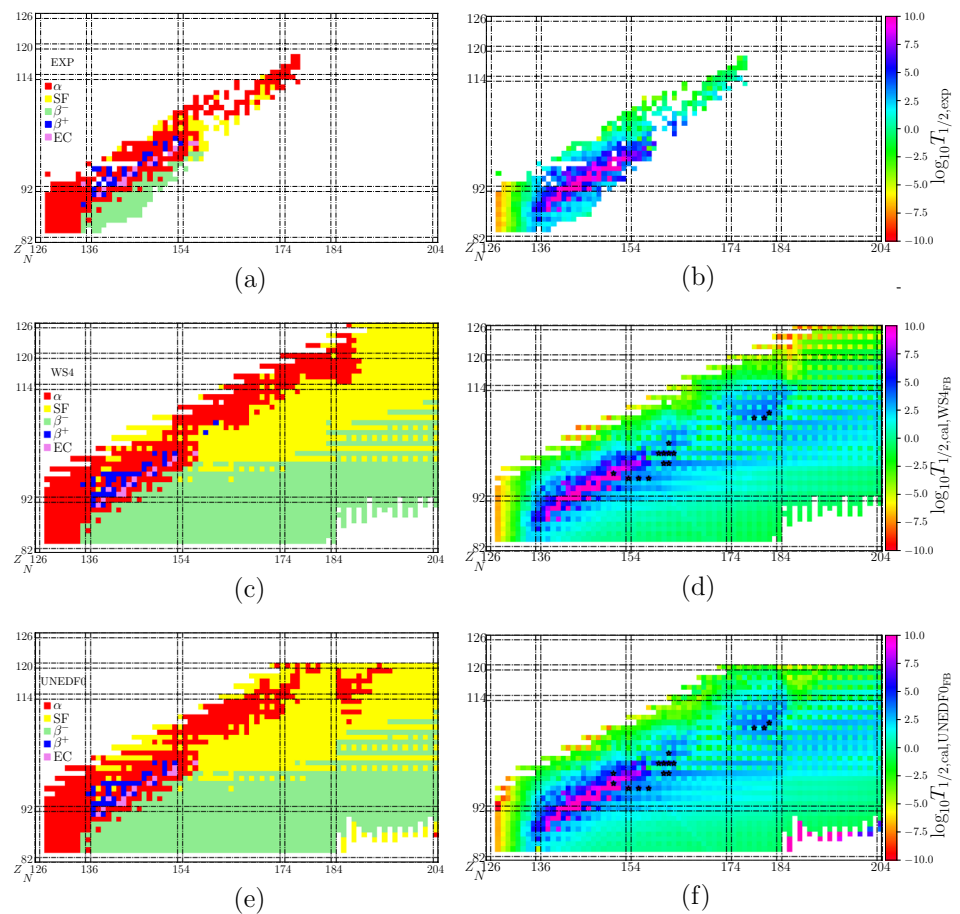
In total, 445 nuclides with measured partial half-lives and branch ratios of the five decay modes were obtained from NUBASE2020 [63]. The dominant decay modes and partial half-lives of the nuclides are illustrated in Fig. 2(a,b). A long-lived  $\alpha$  decay valley from  $^{226}\text{Ra}_{138}$  to  $^{251}\text{Cf}_{153}$  lies between the narrow  $\beta^+/\text{EC}$  decay band and the neutron-rich  $\beta^-$  region. The half-life of the nucleus decreases with increasing distance from this valley. The southwest was dominated by  $\alpha$  decay, whereas the southeast was dominated by  $\beta^-$  decay. In the northwest,  $\beta^+$  decay and EC compete with  $\alpha$  decay and lose after  $Z$  increases. In the northeast,  $\alpha$  decay and SF compete with one other, and the region extending from the  $\alpha$  valley appears to be dominated by the SF. Although the distribution of the dominant decay modes

demonstrates a clear boundary, the minimum partial half-life was smooth.

Among the 445 nuclides considered, 341 (104) nuclides had known (unknown) corresponding decay energies. The nuclides with unmeasured masses were calculated using WS4 [12] and UNEDF0 [13] to estimate the partial half-lives. The results of the RF are presented in Fig. 2(c–f). The calculated results sufficiently agree with the experimental results because the dominant decay mode is correctly described for 431 and 427 (96.9% and 96.0%) nuclei when the RMSE of  $\log_{10} T_{1/2}$  of the dominant decay mode is 0.62 and 0.67, respectively. Nuclides, for which the dominant decay mode was inconsistently described, generally have two competitive decay modes. For example, the  $\alpha$  and SF branch ratios of  $^{255}\text{Rf}$ ,  $^{262}\text{Db}$ , and  $^{286}\text{Fl}$  were approximately 50%. Meanwhile, the liquid drop model trained by RF [62] was also applied to obtain the energies; the model afforded consistent results that are not presented herein.

The  $N - Z = 48$  chain, where the partial half-lives of the  $\alpha$  decay,  $\beta$  decay, and SF are comparable, was used for a specific comparison. The results of the density-dependent cluster model within the anisotropic deformation-dependent surface diffuseness [64], Royer formula [66], modified Swiatecki's formula [22], nuclear liquid drop model [23],

**Fig. 2** (Color online) Dominant decay mode (left panels) and minimum partial half-lives (right panels) of the  $\alpha$  decay,  $\beta^-$  decay,  $\beta^+$  decay, EC, and SF. **a, b** Experimental data in NUBASE2020. **c–f** The results predicted through RF; WS4 [12] and UNEDF0 [13] denote the sources of predicted energies. Specifically, the FB is used to replace the decay energy to learn SF. The nuclides, for which the predicted partial half-life is longer than  $10^4$  s, are marked by a star



and deformed self-consistent Hartree–Fock mean-field with Skyrme forces and pairing correlations [66] were compared with the experimental values; the results are presented in Table 2. The models afforded similar results and deduced a consistent dominant decay mode.

The accuracy of the obtained energy is crucial for half-life calculations. If the calculated energies of WS4 and UNEDF0 replace all the experimental energies, the number with a consistent decay mode compared to the experiment reduces to 72.6% and 64%, respectively, and the RMSE of  $\log_{10} T_{1/2}$  increases to 2.07 and 2.64. The difference in the results obtained using the energies of the two models is owing to the accuracy because the RMSE of the mass of WS4 is approximately 0.3 MeV [12], whereas that of UNEDF0 is approximately 1.45 MeV [13]. This also leads to differences during extrapolation. The consistency rate of the dominant decay mode between the energies calculated using these two models decreases from 82.2% to 66.2%. More accurate and precise measurements of the decay energy will aid in theoretical predictions. In addition, WS4 and UNEDF0 may lose their predictive power after training with machine learning. Training the WS4 and UNEDF0 binding energies with features  $Z, N, \delta,$  and  $P,$  which sufficiently describe the residuals in Ref. [42], improves the energy description but decreases the consistency in the dominant decay mode by several percent, which is considerable compared to the 23.4% rate of the theoretical energies among all nuclides (104/445).

The SF is important for investigating the half-lives of superheavy nuclei. As shown in Fig. 2(c, e), the dominant decay mode of the unknown nuclides is determined in accordance with the competition between the SF,  $\alpha$  decay, and  $\beta^-$  decay. The major competition is between the SF and  $\beta^-$  decay for neutron-rich nuclides, and between the SF and  $\alpha$  decay for neutron-deficient nuclides. Existing experimental data demonstrate a long-lived  $\alpha$  decay region from  $^{226}_{88}\text{Ra}_{138}$  to  $^{251}_{98}\text{Cf}_{153}$ , lying between the  $\beta^+$  and  $\beta^-$  decay regions, and ending with the SF. The proposed models correctly describe this phenomenon. In the long-lived region, after  $N$

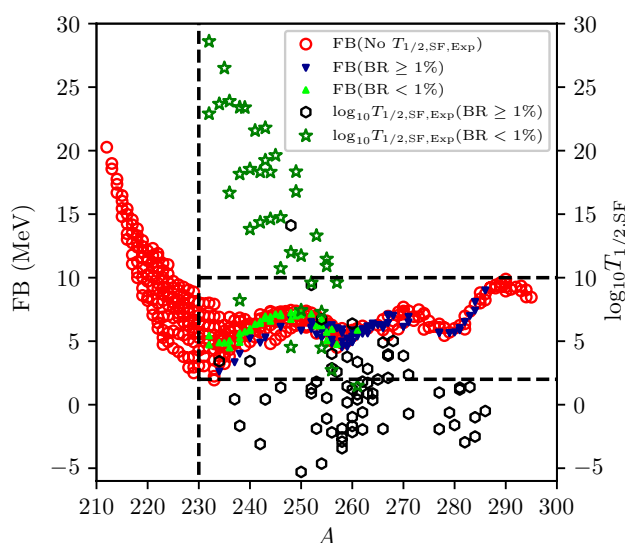


Fig. 3 (Color online) Evolution of  $T_{1/2,SF}$  and FB along the mass number. The datasets are divided according to whether the corresponding  $T_{1/2,SF}$  is measured and whether the branch ratio (BR) of SF is less than 1%

exceeds 154, the blue band shown in Fig. 2(d, f) indicates half-lives of approximately  $10^2$ – $10^7$  s. At the southwest corner of  $Z = 114$  and  $N = 184$ , nuclides in the circle have a longer half-life than those in the surrounding area. This is because of the high FB in this region, which leads to a longer  $T_{1/2,SF}$ . Figure 3 compares the evolution of FB and measured  $T_{1/2,SF}$  along the mass number. The FB decreases with  $A$  before  $A = 230$  and subsequently behaves as a sinusoidal wave oscillating between 2 and 10 MeV. Apparently, an FB threshold exists, below which SF occurs. Nuclides with relatively long  $T_{1/2,SF}$  generally have small SF branch ratios. In addition, the FB of nuclides with SF branch ratios less than 1% were mostly higher than those with SF branch ratios greater than 1%, which implies that the higher the FB, the weaker the SF. However, considering only the nuclides with

Table 2 Comparison of the experimental partial half-lives of the  $N - Z = 48$  chain with the values calculated by different models

Nucl	$\lg T_{\alpha,exp}$	$\lg T_{\alpha,cal}$	$\lg T_{\alpha}^{[64]}$	$\lg T_{\alpha}^{[66]}$	$\lg T_{SF,exp}$	$\lg T_{SF,cal}$	$\lg T_{SF}^{[23]}$	$\lg T_{SF}^{[22]}$	$\lg T_{\beta^+,exp}$	$\lg T_{EC,exp}$	$\lg T_{\beta^+,cal}$	$\lg T_{EC,cal}$	$\lg T_{\beta^+/EC}^{[66]}$
$^{244}\text{Cf}$	3.193	3.298	3.009	3.334	–	–	–	–	–	3.670	–	4.426	3.403
$^{246}\text{Es}$	3.658	4.464	–	–	–	–	–	–	2.698	–	2.213	–	–
$^{248}\text{Fm}$	1.538	1.637	3.358	1.731	4.538	4.678	4.739	5.069	–	–	–	–	2.025
$^{250}\text{Md}$	2.887	2.567	–	–	–	–	–	–	1.764	–	1.809	–	–
$^{252}\text{No}$	0.562	0.541	0.253	0.675	0.897	1.799	1.499	2.119	2.351	–	2.223	–	1.822
$^{254}\text{Lr}$	1.224	1.159	–	–	–	–	–	–	1.627	–	1.577	–	–
$^{256}\text{Rf}$	0.328	0.082	–0.198	0.250	–2.179	–1.382	–1.071	0.519	–	–	–	–	1.898
$^{258}\text{Db}$	0.530	0.037	–	–	–	–	–	–	0.780	–	1.349	–	–
$^{260}\text{Sg}$	–1.768	–1.940	–2.300	–	–2.157	–2.862	–2.811	–2.301	–	–	–	–	–

SF branch ratios of less than 1% or greater than 1%, the correspondence between FB and  $T_{1/2,SF}$  becomes significantly more complex.

The nuclides with partial half-lives predicted to be longer than  $10^4$  s are marked with stars in Figs. 2(d, f), which suggests  $^{250,252,254}\text{Cm}$ ,  $^{260,261}\text{Es}$ ,  $^{261-264}\text{Md}$ , and  $^{265}\text{Lr}$  for future measurements. No experimental value of the half-life of  $^{250}\text{Cm}$  was suggested in NUBASE2020 and was thus extrapolated in this study. In the NNDC, SF was shown to be the dominant decay mode, and its half-life was recommended to be 8300 years, which is relatively long. Although the calculations in this study underestimate the NNDC value, the long half-life and dominant decay mode are reproduced. In addition, the upper limit of the half-life of  $^{252}\text{Cm}$  was proposed to be two days in Ref. [65], which was not updated since then (1966), whereas the current study estimates a half-life of 1.43 days. No experimental half-lives were previously reported for  $^{260,261}\text{Es}$ ,  $^{261-264}\text{Md}$ , and  $^{265}\text{Lr}$ . However, their nearby isotopes have long half-lives, such as  $^{257}\text{Es}$  (7.7 days),  $^{260}\text{Md}$  (31.8 days),  $^{259}\text{Md}$  (1.6 h),  $^{258}\text{Md}$  (51.5 days),  $^{257}\text{Md}$  (5.52 h), and  $^{266}\text{Lr}$  (11 h). Moreover, the Es, Md, and Lr isotopes are located in the extension of the narrow long-lived region from  $^{226}\text{Ra}$  to  $^{251}\text{Cf}$ , substantiating that the Es, Md, and Lr isotopes are candidates with long partial half-lives. Obtaining more measurements is also suggested; for example, the  $^{252}\text{Cm}$  data have not been updated for more than 50 years.

A comparison of all the possible decay channels is limited by the accurate description of each channel and the observed data; note, the SF mechanism remains unclear, such as its dependence on the FB or deformation. The effect of the quadrupole deformation parameter ( $\epsilon_2$ ) [15] on the half-life estimation was then investigated. If the FB is replaced with  $\epsilon_2$  during RF training, more nuclides are predicted to have longer half-lives. Further investigations should be conducted to understand the dominant factors that contribute to the half-life of SF. The FB combines the contributions of multipole deformations and thus presents a stronger quantum effect, as shown in Fig. 2(d, f), compared to  $\epsilon_2$ . Fig. 3 demonstrates that the FB increases when  $Z$  is large; this indicates the competition between the FB and Coulomb repulsion in superheavy nuclides.

The extrapolation stops at the single-neutron (proton) and two-neutron (two-proton) drip lines. The UNEDF0 data set stops at  $Z = 120$ . From the existing region to the neutron-deficient side, the  $\alpha$  decay and SF are predicted to compete. On the neutron-rich side, the calculations predict the  $\beta^-$  decay as the dominant mode, whereas the SF competes for specific nuclides. The latest results of most theoretical calculations of the partial half-lives [17–20, 22, 23, 66–70] indicate that the  $\alpha$  decay mode is dominant for new elements at  $N \leq 184$ . As shown in Fig. 4, the partial half-lives of isotopes with  $Z = 117$ – $122$  were predicted in this study

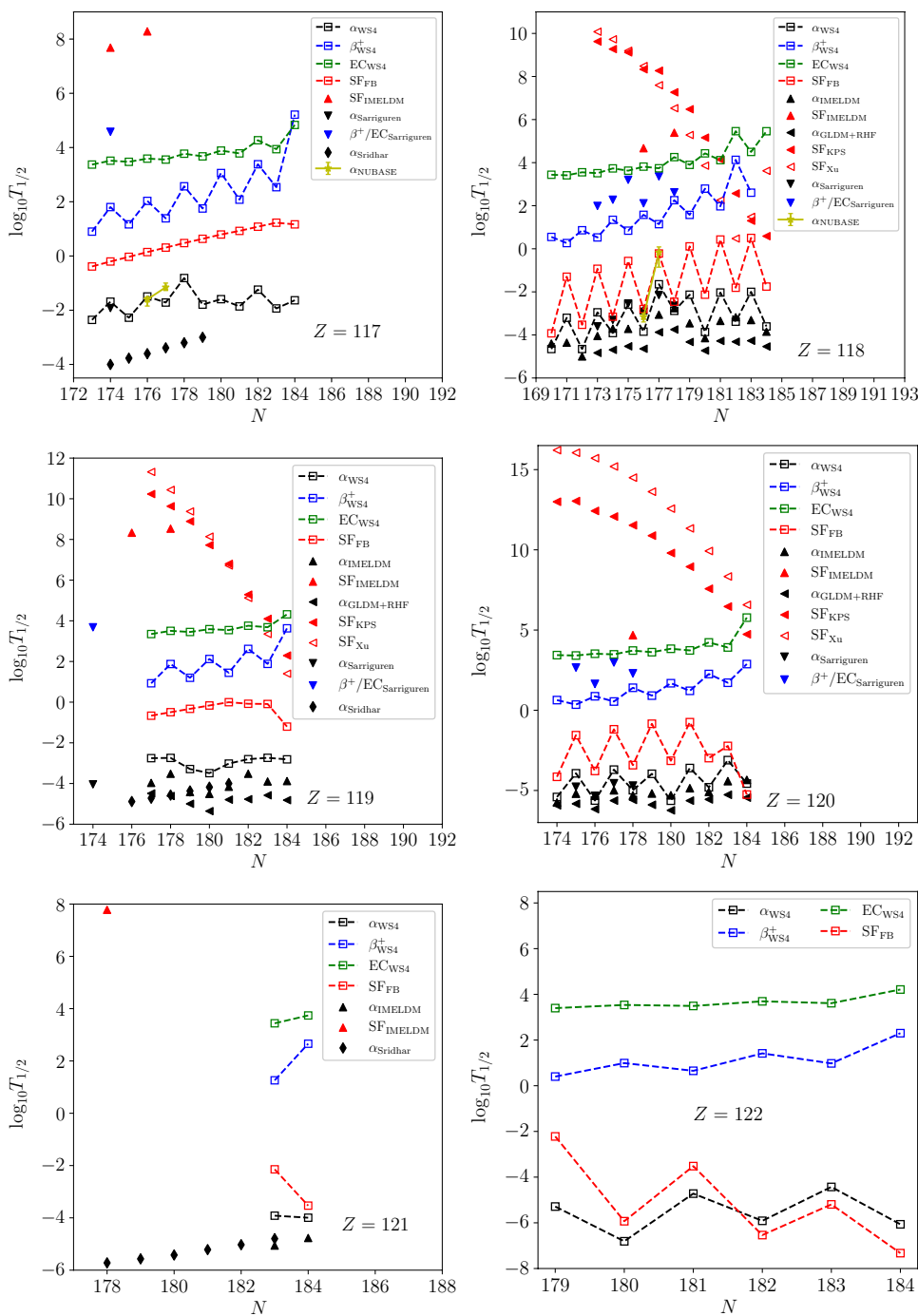
and compared to the corresponding results in Refs. [18–20]. Although the partial half-lives of  $\beta^+$  decay and EC determined in this study were not longer than those indicated in Ref. [20], they remain approximately five orders of magnitude greater than that of  $\alpha$  decay in this region, which does not change the dominant decay mode.

The  $T_{1/2,\alpha}$  values predicted in this study were longer than those indicated in Refs. [18–20]; this does not change the dominant decay mode of odd- $Z$  isotopes but enhances the competition of SF in even- $Z$  isotopes. Furthermore, the prediction in this study demonstrated a strong odd–even staggering of  $T_{1/2,SF}$  of even- $Z$  isotopes. In other words, the  $T_{1/2,SF}$  value of even–even nuclei is several times shorter than its two isotopic neighbors, which differs from the weak or unpredicted odd–even staggering effect obtained by other SF models shown in Fig. 4. Notably, all measured  $T_{1/2,SF}$  values of the even- $Z$  isotopes demonstrate such odd–even staggering. Figure 5 illustrates  $T_{1/2,SF}$  and  $T_{1/2,\alpha}$  of isotopes with  $Z \geq 92$ . For example, when  $Z$  is small in the U, Pu, Cm, and Cf isotopes, SF is not competitive with the  $\alpha$  decay because the Coulomb repulsion is not sufficiently strong. However, when  $Z$  is large, the Coulomb repulsion increases, and this odd–even staggering makes the SF competitive with the  $\alpha$  decay in the even–even nuclides. Thus,  $\alpha$  decay is suggested to be a key signal detected for  $Z = 119$  and  $121$  isotopes, whereas the SF should also be considered for even- $N$  isotopes of  $Z = 120$  and  $122$ . Moreover, odd–even staggering also exists in odd- $Z$  isotopes, which can only be verified by  $^{260-263}\text{Db}$  because the data are limited. Therefore, the odd–even staggering of odd- $Z$  isotopes was not predicted in this study. The DNS model predicted the  $\sigma_{ER}$  value of hundreds of FB for the  $3n$  or  $2n$  channels producing  $^{293}119_{174}$  on the  $^{243}\text{Am}$  target [71], which can be examined for the new facilities of CAFE2 and SHANS2 in Lanzhou [72]. Given the odd–even effect of partial half-lives, nuclide candidates for new superheavy elements still require an analysis based on the cross section and partial half-life.

## 4 Summary

In this study, the decay modes of superheavy nuclei were investigated using the RF algorithm. The partial half-lives of  $\alpha$  decay,  $\beta^-$  decay,  $\beta^+$  decay, as well as EC, and SF were studied and compared. The dominance of  $\alpha$  decay in the neutron-deficient region was relatively evident.  $\beta^-$  decay is predicted to be dominant in the neutron-rich regions. The SF contributes to a long-lived circle at the southwest corner of  $Z = 114$  and  $N = 184$ . A more accurate and precise measurement of the nuclear mass and decay energy can improve the prediction of the decay mode. The odd–even effect of the SF was observed in even- $Z$  nuclides. Combined with the strong Coulomb repulsion, the SF and  $\alpha$  decay became

**Fig. 4** (Color online) Comparison of the partial half-lives of isotopes with  $Z = 117$ – $122$ . IMELDM is extracted from Ref. [18], GLDM+RHF, KPS, and Xu are extracted from [19], Sarriguren is extracted from Ref. [20], Sridhar is extracted from Ref. [69]



competitive in even–even nuclides. Thus, the  $\alpha$  decay is suggested to be a key probe of isotopes with  $Z = 119$  and  $121$ , whereas the competition of SF should be considered in even–even isotopes with  $Z = 120$  and  $122$ .

$^{250,252,254}\text{Cm}$ ,  $^{260,261}\text{Es}$ ,  $^{261-264}\text{Md}$ , and  $^{265}\text{Lr}$  with half-lives predicted to be longer than  $10^4$  s were suggested for

future measurements. The SF, influenced by the fission barrier and Coulomb repulsion, leads to a long-lived region during extrapolation. The results of this study indicate that research regarding SF, especially beyond  $^{286}\text{Fl}$ , which is currently the heaviest nuclide with a significant SF branch ratio, is critical for performing studies on new facilities, such as CAFE2 and SHANS2 in Lanzhou.

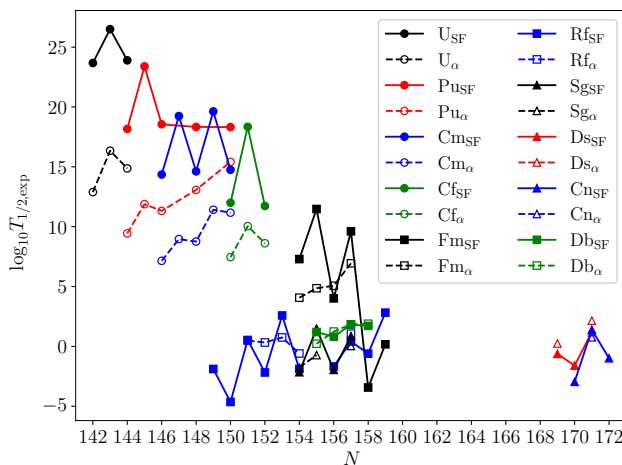


**Fig. 5** (Color online) Odd–even staggering of  $T_{1/2, SF}$  of U, Pu, Cm, Cf, Fm, Rf, Sg, Ds, Cn, and Db isotopes and comparison with  $T_{1/2, \alpha}$

**Acknowledgements** The authors acknowledge the useful discussion with Professors Zai-Guo Gan, Zhong-Zhou Ren, and Zhi-Yuan Zhang.

**Author Contributions** All authors contributed to the study conception and design. Material preparation, data collection and analysis were performed by Bo-Shuai Cai. The first draft of the manuscript was written by Bo-Shuai Cai, and all authors commented on previous versions of the manuscript. All authors read and approved the final manuscript.

**Data Availability** The data that support the findings of this study are openly available in Science Data Bank at <https://www.doi.org/10.57760/sciencedb.12102> and <https://cstr.cn/31253.11.sciencedb.12102>.

## Declarations

**Conflict of interest** Cen-Xi Yuan is an editorial board member for Nuclear Science and Techniques and was not involved in the editorial review, or the decision to publish this article. All authors declare that there are no competing interests.

## References

1. W. Nazarewicz, The limits of nuclear mass and charge. *Nat. Phys.* **14**, 537 (2018). <https://doi.org/10.1038/s41567-018-0163-3>
2. J. Erler, N. Birge, M. Kortelainen et al., The limits of the nuclear landscape. *Nature* **486**, 509 (2012). <https://doi.org/10.1038/nature11188>
3. T. Otsuka, A. Gade, O. Sorlin et al., Evolution of shell structure in exotic nuclei. *Rev. Mod. Phys.* **92**, 015002 (2020). <https://doi.org/10.1103/RevModPhys.92.015002>
4. T. Otsuka, T. Suzuki, M. Honma et al., Novel features of nuclear forces and shell evolution in exotic nuclei. *Phys. Rev. Lett.* **104**, 012501 (2010). <https://doi.org/10.1103/PhysRevLett.104.012501>
5. A. Ozawa, T. Kobayashi, T. Suzuki et al., New magic number,  $N = 16$ , near the neutron drip line. *Phys. Rev. Lett.* **84**, 5493 (2000). <https://doi.org/10.1103/PhysRevLett.84.5493>
6. N.A. Smirnova, B. Bally, K. Heyde et al., Shell evolution and nuclear forces. *Phys. Lett. B* **686**, 109 (2010). <https://doi.org/10.1016/j.physletb.2010.02.051>

7. M. Duer, T. Aumann, R. Gernhäuser et al., Observation of a correlated free four-neutron system. *Nature* **606**, 678 (2022). <https://doi.org/10.1038/s41586-022-04827-6>
8. J.G. Li, N. Michel, B.S. Hu et al., *Abinitio* no-core Gamow shell-model calculations of multineutron systems. *Phys. Rev. C* **100**, 054313 (2019). <https://doi.org/10.1103/PhysRevC.100.054313>
9. Y. Jin, C.Y. Niu, K.W. Brown et al., First observation of the four-proton unbound nucleus  $^{18}\text{Mg}$ . *Phys. Rev. Lett.* **127**, 262502 (2021). <https://doi.org/10.1103/PhysRevLett.127.262502>
10. S. Hofmann, G. Münzenberg, The discovery of the heaviest elements. *Rev. Mod. Phys.* **72**, 733 (2000). <https://doi.org/10.1103/RevModPhys.72.733>
11. S.A. Giuliani, Z. Matheson, W. Nazarewicz et al., *Colloquium*: superheavy elements: oganesson and beyond. *Rev. Mod. Phys.* **91**, 011001 (2019). <https://doi.org/10.1103/RevModPhys.91.011001>
12. N. Wang, M. Liu, X. Wu et al., Surface diffuseness correction in global mass formula. *Phys. Lett. B* **734**, 215 (2014). <https://doi.org/10.1016/j.physletb.2014.05.049>
13. M. Kortelainen, T. Lesinski, J. Moré et al., Nuclear energy density optimization. *Phys. Rev. C* **82**, 024313 (2010). <https://doi.org/10.1103/PhysRevC.82.024313>
14. W.D. Myers, Development of the semiempirical droplet model. *At. Data Nucl. Data Tables* **17**, 411 (1976). [https://doi.org/10.1016/0092-640X\(76\)90030-9](https://doi.org/10.1016/0092-640X(76)90030-9)
15. P. Möller, A.J. Sierk, T. Ichikawa et al., Nuclear ground-state masses and deformations: FRDM(2012). *Atom. Data Nucl. Data* **109–110**, 1 (2016). <https://doi.org/10.1016/j.adt.2015.10.002>
16. S. Goriely, N. Chamel, and J. Pearson, Hartree-Fock-Bogoliubov nuclear mass model with 0.50 MeV accuracy based on standard forms of Skyrme and pairing functionals. *Phys. Rev. C* **88**, 061302 (2013). <https://doi.org/10.1103/PhysRevC.88.061302>
17. G. Saxena, A. Jain, P.K. Sharma, A new empirical formula for  $\alpha$ -decay half-life and decay chains of  $Z = 120$  isotopes. *Phys. Scr.* **96**, 125304 (2021). <https://doi.org/10.1088/1402-4896/ac1a4d>
18. J.P. Cui, Y.H. Gao, Y.Z. Wang et al., Improved effective liquid drop model for  $\alpha$ -decay half-lives. *Nucl. Phys. A* **1017**, 122341 (2022). <https://doi.org/10.1016/j.nuclphysa.2021.122341>
19. C. He, Z.M. Niu, X.J. Bao et al., Research on  $\alpha$ -decay for the superheavy nuclei with  $Z = 118–120$ . *Chin. Phys. C* **46**, 054102 (2022). <https://doi.org/10.1088/1674-1137/ac4c3a>
20. P. Sarriguren, Self-consistent calculations of electron-capture decays in  $Z = 118, 119$ , and  $120$  superheavy isotopes. *Phys. Lett. B* **815**, 136149 (2021). <https://doi.org/10.1016/j.physletb.2021.136149>
21. Y.F. Gao, B.S. Cai, C.X. Yuan, Investigation of  $\beta^-$ -decay half-life and delayed neutron emission with uncertainty analysis. *Nucl. Sci. Tech.* **34**, 9 (2023). <https://doi.org/10.1007/s41365-022-01153-4>
22. X.J. Bao, S.Q. Guo, H.F. Zhang et al., Competition between  $\alpha$ -decay and spontaneous fission for superheavy nuclei. *J. Phys. G Nucl. Part. Phys.* **42**, 085101 (2015). <https://doi.org/10.1088/0954-3899/42/8/085101>
23. A. Soylu, Search for decay modes of heavy and superheavy nuclei. *Chin. Phys. C* **43**, 074102 (2019). <https://doi.org/10.1088/1674-1137/43/7/074102>
24. B.S. Cai, C.X. Yuan, Theoretical description of the decay width of neutron emission in light nuclei. *Chin. Sci. Bull.* **67**, 2782–2789 (2022). <https://doi.org/10.1360/TB-2022-0151>. (in Chinese)
25. Z. Zhang, C. Yuan, C. Qi et al., Extended R-matrix description of two-proton radioactivity. *Phys. Lett. B* **838**, 137740 (2023). <https://doi.org/10.1016/j.physletb.2023.137740>
26. P. Mehta, M. Bukov, C.-H. Wang et al., A high-bias, low-variance introduction to machine learning for physicists. *Phys. Rep.* **810**, 1 (2019). <https://doi.org/10.1016/j.physrep.2019.03.001>
27. W.-B. He, Y.-G. Ma, L.-G. Pang et al., High-energy nuclear physics meets machine learning. *Nucl. Sci. Tech.* **34**, 88 (2023). <https://doi.org/10.1007/s41365-023-01233-z>

28. X.-K. Du, P. Guo, X.-H. Wu et al., Examination of machine learning for assessing physical effects: learning the relativistic continuum mass table with kernel ridge regression. *Chin. Phys. C* **47**, 074108 (2023). <https://doi.org/10.1088/1674-1137/acc791>
29. W. He, Q. Li, Y. Ma et al., Machine learning in nuclear physics at low and intermediate energies. *Sci. Chin. Phys. Mech. Astron.* **66**, 282001 (2023). <https://doi.org/10.1007/s11433-023-2116-0>
30. W.-J. Xie, Z.-W. Ma, J.-H. Guo, Bayesian inference of the crust-core transition density via the neutron-star radius and neutron-skin thickness data. *Nucl. Sci. Tech.* **34**, 91 (2023). <https://doi.org/10.1007/s41365-023-01239-7>
31. Q.-F. Song, L. Zhu, H. Guo et al., Verification of neutron-induced fission product yields evaluated by a tensor decomposition model in transport-burnup simulations. *Nucl. Sci. Tech.* **34**, 32 (2023). <https://doi.org/10.1007/s41365-023-01176-5>
32. Z.A. Wang, J.C. Pei, Y.J. Chen et al., Bayesian approach to heterogeneous data fusion of imperfect fission yields for augmented evaluations. *Phys. Rev. C* **106**, L021304 (2022). <https://doi.org/10.1103/PhysRevC.106.L021304>
33. Q. Song, L. Zhu, B. Cai et al., Image processing of isotope yield in neutron-induced fission. *Phys. Rev. C* **107**, 044609 (2023). <https://doi.org/10.1103/PhysRevC.107.044609>
34. Z.-A. Wang, J. Pei, Optimizing multilayer Bayesian neural networks for evaluation of fission yields. *Phys. Rev. C* **104**, 064608 (2021). <https://doi.org/10.1103/PhysRevC.104.064608>
35. Z.-A. Wang, J. Pei, Y. Liu et al., Bayesian evaluation of incomplete fission yields. *Phys. Rev. Lett.* **123**, 122501 (2019). <https://doi.org/10.1103/PhysRevLett.123.122501>
36. Y.-D. Zeng, J. Wang, R. Zhao et al., Decomposition of fissile isotope antineutrino spectra using convolutional neural network. *Nucl. Sci. Tech.* **34**, 79 (2023). <https://doi.org/10.1007/s41365-023-01229-9>
37. K.-F. Pu, H.-L. Li, H.-L. Lv et al., Solving Schrodinger equations using a physically constrained neural network. *Chin. Phys. C* **47**, 054104 (2023). <https://doi.org/10.1088/1674-1137/acc518>
38. R. Seifert, M. Weber, E. Kocakavuk et al., Artificial intelligence and machine learning in nuclear medicine: future perspectives. *Semin. Nucl. Med.* **51**, 170 (2021). <https://doi.org/10.1053/j.semnuclmed.2020.08.003>
39. F.-D. Qin, H.-Y. Luo, Z.-Z. He et al., Counting of alpha particle tracks on imaging plate based on a convolutional neural network. *Nucl. Sci. Tech.* **34**, 37 (2023). <https://doi.org/10.1007/s41365-023-01190-7>
40. A. Boehnlein, M. Diefenthaler, C. Fanelli et al., *Colloquium: machine learning in nuclear physics*. *Rev. Mod. Phys.* **94**, 031003 (2022). <https://doi.org/10.1103/RevModPhys.94.031003>
41. R. Utama, J. Piekarewicz, H.B. Prosper, Nuclear mass predictions for the crustal composition of neutron stars: a Bayesian neural network approach. *Phys. Rev. C* **93**, 014311 (2016). <https://doi.org/10.1103/PhysRevC.93.014311>
42. Z.M. Niu, H.Z. Liang, Nuclear mass predictions based on Bayesian neural network approach with pairing and shell effects. *Phys. Lett. B* **778**, 48 (2018). <https://doi.org/10.1016/j.physletb.2018.01.002>
43. Z.M. Niu, J.Y. Fang, Y.F. Niu, Comparative study of radial basis function and Bayesian neural network approaches in nuclear mass predictions. *Phys. Rev. C* **100**, 054311 (2019). <https://doi.org/10.1103/PhysRevC.100.054311>
44. R. Utama, W.-C. Chen, J. Piekarewicz, Nuclear charge radii: density functional theory meets Bayesian neural networks. *J. Phys. G Nucl. Part. Phys.* **43**, 114002 (2016). <https://doi.org/10.1088/0954-3899/43/11/114002>
45. D. Wu, C.L. Bai, H. Sagawa et al., Calculation of nuclear charge radii with a trained feed-forward neural network. *Phys. Rev. C* **102**, 054323 (2020). <https://doi.org/10.1103/PhysRevC.102.054323>
46. X.-X. Dong, R. An, J.-X. Lu et al., Novel Bayesian neural network based approach for nuclear charge radii. *Phys. Rev. C* **105**, 014308 (2022). <https://doi.org/10.1103/PhysRevC.105.014308>
47. M. Carnini, A. Pastore, Trees and forests in nuclear physics. *J. Phys. G Nucl. Part. Phys.* **47**, 082001 (2020). <https://doi.org/10.1088/1361-6471/ab92e3>
48. L. Breiman, Random forests. *Mach. Learn.* **45**, 5 (2001). <https://doi.org/10.1023/A:1010933404324>
49. C. Qi, F.R. Xu, R.J. Liotta et al., Microscopic mechanism of charged-particle radioactivity and generalization of the Geiger–Nuttall law. *Phys. Rev. C* **80**, 044326 (2009). <https://doi.org/10.1103/PhysRevC.80.044326>
50. C. Qi, F.R. Xu, R.J. Liotta et al., Universal decay law in charged-particle emission and exotic cluster radioactivity. *Phys. Rev. Lett.* **103**, 072501 (2009). <https://doi.org/10.1103/PhysRevLett.103.072501>
51. Z.Z. Ren, C. Xu, Spontaneous fission half-lives of heavy nuclei in ground state and in isomeric state. *Nucl. Phys. A* **759**, 64 (2005). <https://doi.org/10.1016/j.nuclphysa.2005.04.019>
52. C. Xu, Z.Z. Ren, Y.Q. Guo, Competition between  $\alpha$  decay and spontaneous fission for heavy and superheavy nuclei. *Phys. Rev. C* **78**, 044329 (2008). <https://doi.org/10.1103/PhysRevC.78.044329>
53. K.P. Santhosh, R.K. Biju, S. Sahadevan, Semi-empirical formula for spontaneous fission half life time. *Nucl. Phys. A* **832**, 220 (2010). <https://doi.org/10.1016/j.nuclphysa.2009.10.160>
54. K.P. Santhosh, C. Nithya, T.A. Jose, Decay modes of superheavy nuclei using a modified generalized liquid drop model and a mass-inertia-dependent approach for spontaneous fission. *Phys. Rev. C* **104**, 024617 (2021). <https://doi.org/10.1103/PhysRevC.104.024617>
55. G. Royer, Alpha emission and spontaneous fission through quasi-molecular shapes. *J. Phys. G: Nucl. Part. Phys.* **26**, 1149 (2000). <https://doi.org/10.1088/0954-3899/26/8/305>
56. J. Suhonen, *From Nucleons to Nucleus: Concepts of Microscopic Nuclear Theory* (Springer, Berlin Heidelberg, 2007), pp.163–169
57. M. Wang, W.J. Huang, F.G. Kondev et al., The AME 2020 atomic mass evaluation (II) Tables, graphs and references. *Chinese Phys. C* **45**, 030003 (2021). <https://doi.org/10.1088/1674-1137/abddaf>
58. B. Cai, G. Chen, J. Xu et al.,  $\alpha$ -decay half-life estimation and uncertainty analysis. *Phys. Rev. C* **101**, 054304 (2020). <https://doi.org/10.1103/PhysRevC.101.054304>
59. B. Cai, G. Chen, C. Yuan et al., Shell-model study on properties of proton dripline nuclides with  $Z, N = 30\text{--}50$  including uncertainty analysis. *Chinese Phys. C* **46**, 084104 (2022). <https://doi.org/10.1088/1674-1137/ac6cd7>
60. F. Pedregosa, G. Varoquaux, A. Gramfort et al., Scikit-learn: machine learning in python. *J. Mach. Learn. Res.* **12**, 2825 (2011). <https://doi.org/10.5555/1953048.2078195>
61. P. Möller, A.J. Sierk, T. Ichikawa et al., Fission barriers at the end of the chart of the nuclides. *Phys. Rev. C* **91**, 024310 (2015). <https://doi.org/10.1103/PhysRevC.91.024310>
62. B. Cai, T. Yu, X. Lin et al., Investigation of nuclear binding energy and charge radius based on random forest algorithm. *At. Energ. Sci. Technol.* **57**, 704 (2023). <https://doi.org/10.7538/yzk.2022.youxian.0780>
63. F.G. Kondev, M. Wang, W.J. Huang et al., The NUBASE2020 evaluation of nuclear physics properties. *Chinese Phys. C* **45**, 030001 (2021). <https://doi.org/10.1088/1674-1137/abddae>
64. Z. Wang, D. Bai, Z.Z. Ren, Improved density-dependent cluster model in  $\alpha$ -decay calculations within anisotropic deformation-dependent surface diffuseness. *Phys. Rev. C* **105**, 024327 (2022). <https://doi.org/10.1103/PhysRevC.105.024327>
65. Combined Radiochemistry Group, Nuclear decay properties of heavy nuclides produced in thermonuclear explosions-par and barbel events. *Phys. Rev.* **148**, 1192 (1966). <https://doi.org/10.1103/PhysRev.148.1192>

66. P. Sarriguren, Competition between weak and  $\alpha$ -decay modes in superheavy nuclei. *Phys. Rev. C* **105**, 014312 (2022). <https://doi.org/10.1103/PhysRevC.105.014312>
67. C. Xu, X. Zhang, Z.Z. Ren, Stability of superheavy nuclei against  $\alpha$ -decay and spontaneous fission. *Nucl. Phys. A* **898**, 24 (2013). <https://doi.org/10.1016/j.nuclphysa.2012.12.022>
68. J.H. Liu, S.Q. Guo, X.J. Bao et al., Predictions of decay modes for the superheavy nuclei most suitable for synthesis. *Chin. Phys. C* **41**, 074106 (2017). <https://doi.org/10.1088/1674-1137/41/7/074106>
69. K.N. Sridhar, H.C. Manjunatha, H.B. Ramalingam, Search for possible fusion reactions to synthesize the superheavy element  $Z = 121$ . *Phys. Rev. C* **98**, 064605 (2018). <https://doi.org/10.1103/PhysRevC.98.064605>
70. T. Sahoo, S.K. Patra, Search for the stable isotopes for  $Z = 119$  and 121 superheavy elements using relativistic mean field model. *Phys. Scr.* **95**, 085302 (2020). <https://doi.org/10.1088/1402-4896/ab98b8>
71. F. Li, L. Zhu, Z.-H. Wu et al., Predictions for the synthesis of superheavy elements  $Z = 119$  and 120. *Phys. Rev. C* **98**, 014618 (2018). <https://doi.org/10.1103/PhysRevC.98.014618>
72. L. N. Sheng, Q. Hu, H. Jia et al., Ion-optical design and multiparticle tracking in 3D magnetic field of the gas-filled recoil separator SHANS2 at CAFE2. *Nucl. Instrum. Methods Phys. Res. A* **1004**, 165348 (2021). <https://doi.org/10.1016/j.nima.2021.165348>

Springer Nature or its licensor (e.g. a society or other partner) holds exclusive rights to this article under a publishing agreement with the author(s) or other rightsholder(s); author self-archiving of the accepted manuscript version of this article is solely governed by the terms of such publishing agreement and applicable law.